

Communication

Reverse Water Gas Shift versus Carbon Dioxide Electro-Reduction: The Reaction Pathway Responsible for Carbon Monoxide Production in Solid Oxide Co-Electrolysis Cells

Anders S. Nielsen ^{1,2}, Brant A. Peppley ³ and Odne S. Burheim ^{2,*} 

¹ Department of Mechanical and Materials Engineering, Queen's University, 130 Stuart Street, Kingston, ON K7L 2V9, Canada; anders.nielsen@queensu.ca

² Department of Energy and Process Engineering, Norwegian University of Science and Technology, NO-7491 Trondheim, Norway

³ Department of Chemical Engineering, Queen's University, 19 Division Street, Kingston, ON K7L 2N9, Canada; peppley@queensu.ca

* Correspondence: burheim@ntnu.no; Tel.: +47-917-078-56

Abstract: Solid oxide co-electrolysis cells can utilize renewable energy sources for the conversion of steam and carbon dioxide into valuable chemicals and feedstocks. An important challenge in the analysis of these devices is understanding the reaction pathway(s) that govern carbon monoxide generation. Studies in which co-electrolysis polarization lies between those of pure steam and pure carbon dioxide electrolysis suggest that carbon dioxide electro-reduction (CO₂ER) and the reverse water gas shift (RWGS) reaction are both contributors to CO generation. However, experiments in which co-electrolysis polarization overlaps that of pure steam electrolysis propose that the RWGS reaction dominates CO production and CO₂ER is negligible. Supported by dimensional analysis, thermodynamics, and reaction kinetics, this work elucidates the reasons for which the latter conclusion is infeasible, and provides evidence for why the observed overlap between co-electrolysis and pure steam electrolysis is a result of the slow kinetics of CO₂ER in comparison to that of steam, with the RWGS reaction being inconsequential. For sufficiently thin cathode current collectors, we reveal that CO₂ER is dominant over the RWGS reaction, while the rate of steam electro-reduction is much higher than that of carbon dioxide, which causes the co-electrolysis and pure steam electrolysis polarization curves to overlap. This is contrary to what has been proposed in previous experimental analyses. Ultimately, this work provides insight into how to design solid oxide co-electrolysis cells such that they can exploit a desired reaction pathway in order to improve their efficiency and product selectivity.

Keywords: solid oxide electrolysis cell; solid oxide co-electrolysis; dimensional analysis; thermodynamics; electrochemical kinetics



Citation: Nielsen, A.S.; Peppley, B.A.; Burheim, O.S. Reverse Water Gas Shift versus Carbon Dioxide Electro-Reduction: The Reaction Pathway Responsible for Carbon Monoxide Production in Solid Oxide Co-Electrolysis Cells. *Energies* **2023**, *16*, 5781. <https://doi.org/10.3390/en16155781>

Academic Editors: Antonino S. Arico and Tao Wei

Received: 16 May 2023

Revised: 15 June 2023

Accepted: 2 August 2023

Published: 3 August 2023



Copyright: © 2023 by the authors. Licensee MDPI, Basel, Switzerland. This article is an open access article distributed under the terms and conditions of the Creative Commons Attribution (CC BY) license (<https://creativecommons.org/licenses/by/4.0/>).

1. Introduction

Solid oxide co-electrolysis cells (SOco-ECs) are a promising technology with the capacity to convert CO₂ and steam into syngas (a mixture of H₂ and CO) using renewable and intermittent sources of energy [1–3]. The produced syngas can be delivered to Fischer-Tropsch reactors to generate liquid synthetic fuel and polymers [4,5], which can therefore alleviate society's dependence on fossil fuels and conventional means of manufacturing plastics [6]. A comprehensive overview of the background, application, and importance of SOco-ECs can be found in Refs. [7,8]. One of the key challenges in the analysis and understanding of SOco-ECs is determining the reaction pathway(s) responsible for CO production [7]. Researchers in previous electrochemical analyses have observed different contributions of the reverse water gas shift (RWGS) reaction:



and carbon dioxide electro-reduction (CO₂ER):



alongside steam electro-reduction (H₂OER) to generate hydrogen:



resulting in conflicting arguments in terms of the co-electrolysis reaction pathways [7]. Some researchers have suggested that CO generation is largely attributed to the RWGS reaction [9,10], since the polarization curves of pure steam electrolysis and co-electrolysis overlap each other. Therefore, they surmised that CO₂ER is inconsequential to CO production. Conversely, other studies have shown that the polarization curves corresponding to co-electrolysis lie between those of pure steam and pure carbon dioxide electrolysis [11–13], thus indicating the RWGS reaction and CO₂ER are both contributors [14,15]. Both hypotheses may be plausible, and their different findings could be a result of experiments having been performed in different transport regimes (i.e., diffusion limited versus reaction limited). It is important to develop an understanding of the reaction pathways that govern the generation of CO, since they have a significant impact on the energy demands to perform CO₂ER and H₂OER.

Numerical models of SOco-ECs have been developed to make sense of the results discussed above, but have also yielded varying conclusions. Researchers have determined that CO₂ER is the predominant mechanism for CO generation [16], while others have concluded the RWGS reaction is the dominant pathway [17]. Additionally, Luo et al. [18] and Ni [19] revealed the RWGS reaction can play a significant role, but can transition to consuming carbon monoxide, depending on the operating temperature, inlet gas composition, and flow velocity. Luo et al. conducted additional numerical analyses to investigate how the microstructural properties [20] and thickness [21] of the cathode affect the contribution of electrochemical and heterogeneous chemical reactions. The study revealed that using a cathode with a thickness of 700 μm leads to a contribution from both CO₂ER and the RWGS reaction, while, on the other hand, they suggested that employing a cathode with a thickness of ~30 μm results in CO production through only the RWGS reaction. The latter conclusion was based on the observation that the polarization curves of co-electrolysis and pure steam electrolysis overlap with each other. This latter explanation is counter-intuitive, however, since reducing the thickness of the cathode current collector decreases the amount of catalyst available to facilitate the RWGS reaction. Hence, we believe that reducing the thickness of the cathode current collector makes the RWGS reaction negligible and promotes CO₂ER, therefore causing the polarization curves of co-electrolysis and pure steam electrolysis to overlap each other.

In this work, we develop a physics-based approach to untangle the different behaviour of SOco-ECs reported in previous experiments. A dimensional analysis of the reaction rates corresponding to CO production is initially undertaken to reveal how the contribution of the RWGS reaction and CO₂ER scale with the thickness of the cathode current collector, and we further demonstrate the thickness at which the RWGS reaction is negligible. We then apply the first and second laws of thermodynamics to illustrate the conditions required for the polarization curves of co-electrolysis and pure steam electrolysis to overlap each other. This is followed by a comparison of the kinetics of CO₂ER and H₂OER using Butler-Volmer kinetics. This analysis is intended to provide an enhanced understanding of the behaviour of SOco-ECs, and can help designers make informed decisions on how to construct a cell to exploit a desired reaction pathway in order to reduce the electrical work input.

2. Theoretical Formulation and Experimental Comparison

The current approach is based on the SOco-EC illustrated in Figure 1, which is valid for planar, radial, and tubular systems, wherein steam, carbon dioxide, hydrogen, and carbon

monoxide are supplied to the cathode channel with inlet molar flow rates $J_i^{c,in}$. Steam and carbon dioxide are subsequently transported through the cathode current collector, towards the triple phase boundary, at which point they are electrochemically reduced to generate hydrogen and carbon monoxide, according to reactions (1) and (2) in Figure 1. Since steam, carbon dioxide, hydrogen, and carbon monoxide co-exist in the Ni-YSZ cathode current collector, the RWGS reaction can also occur (reaction (3) in Figure 1), while it is assumed in this analysis that the influence of other possible reactions is negligible. Furthermore, we make the assumption that electrochemical reactions take place at the interface between the electrolyte and cathode current collector [22–25], and we assume that both electrochemical and chemical kinetics occur within a single, rate-determining step. However, when examining a specific cell, it may become necessary to consider the distribution of electrochemical reactions within the active catalyst layers. It is crucial to ensure that these layers are sufficiently thin so that treating the triple phase boundary as an interface remains valid.

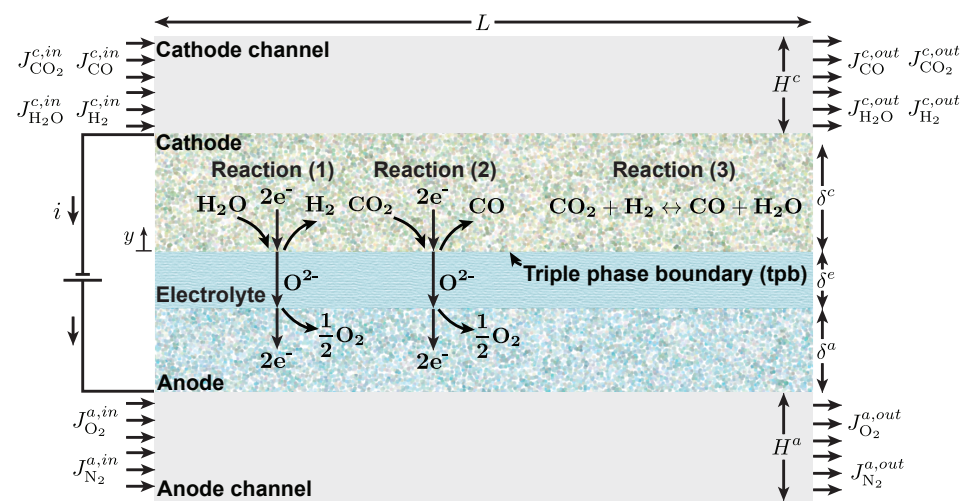


Figure 1. Schematic of a SOco-EC of length L , cathode channel height H^c , cathode thickness δ^c , electrolyte thickness δ^e , anode thickness δ^a , and anode channel height H^a . Reactions considered in the cathode are (1) H₂OER; (2) CO₂ER; and (3) the RWGS reaction.

2.1. Carbon Monoxide Reaction Pathways

The two reaction pathways under investigation are the heterogeneous RWGS reaction in the cathode current collector and CO₂ER at the triple phase boundary. The rate of production of carbon monoxide can be determined by evaluating its utilization factor, which is characterized as the difference between the inlet and outlet molar flow rates across the length of a cell divided by the inlet value:

$$U_{CO}^c = \frac{J_{CO}^{c,in} - J_{CO}^{c,out}}{J_{CO}^{c,in}} = - \underbrace{\frac{LW \int_0^{\delta^c} R_{RWGS}^c dy}{WH^c \bar{V}^{c,in} c_{CO}^{c,in}}}_{U_{CO,RWGS}^c} - \underbrace{\frac{LW i_{CO_2}}{n_{CO_2} F WH^c \bar{V}^{c,in} c_{CO}^{c,in}}}_{U_{CO,elec}^c} \quad (4)$$

where U_{CO}^c is the utilization factor of carbon monoxide, $J_{CO}^{c,in}$ and $J_{CO}^{c,out}$ are its inlet and outlet molar flow rates, respectively, L is the length of the cell, W is its width, H^c is the height of the cathode channel, δ^c is the thickness of the cathode current collector, $\bar{V}^{c,in}$ is the average inlet flow velocity, $c_{CO}^{c,in}$ is the inlet concentration, R_{RWGS}^c is the RWGS reaction rate, n_{CO_2} is the number of electrons transferred in CO₂ER, F is the Faraday constant, i_{CO_2} is the current density corresponding to CO₂ER, $U_{CO,RWGS}^c$ is the utilization factor of carbon monoxide due to the RWGS reaction, and $U_{CO,elec}^c$ is that corresponding to CO₂ER. Carbon monoxide utilization due to the RWGS reaction and CO₂ER are written as negative terms in Equation (4), since both reaction pathways produce CO (i.e., negative utilization).

For the RWGS reaction rate, R_{RWGS}^c , we utilize the expression derived by Haberman and Young [26], which is expressed as:

$$R_{RWGS}^c = k_{RWGS}^c R^2 T^2 (c_{CO_2} c_{H_2} - c_{H_2O} c_{CO} / K_{RWGS}) \quad (5)$$

where k_{RWGS}^c is the RWGS reaction rate constant, R is the universal gas constant, T is the operating temperature, K_{RWGS} is the reaction equilibrium constant, and c_i is the concentration of component i . The current density corresponding to CO₂ER can be evaluated using the concentration gradient at the triple phase boundary (tpb), according to:

$$i_{CO_2} = n_{CO_2} F D_{CO_2} \left. \frac{dc_{CO_2}}{dy} \right|_{y=tpb} \quad (6)$$

where D_{CO_2} is the effective diffusion coefficient in the cathode current collector. Details for how to compute D_{CO_2} is provided in Supplementary Note S1 and Supplementary Table S1 lists the resultant values. We now introduce the following dimensionless parameters: $\tilde{y} \equiv y/\delta^c$ and $\tilde{c}_i \equiv c_i/c_{i,tot}^{c,in}$ and substitute Equations (5) and (6) into Equation (4) to yield:

$$U_{CO}^c = - \underbrace{\frac{L k_{RWGS}^c R^2 T^2 c_{tot}^{c,in} \delta^c}{H^c \bar{V}^{c,in} \tilde{c}_{CO}^{c,in}} \int_0^1 (\tilde{c}_{CO_2} \tilde{c}_{H_2} - \tilde{c}_{H_2O} \tilde{c}_{CO} / K_{RWGS}) d\tilde{y}}_{U_{CO,RWGS}^c} - \underbrace{\frac{L D_{CO_2}}{H^c \bar{V}^{c,in} \delta^c \tilde{c}_{CO}^{c,in}} \left. \frac{d\tilde{c}_{CO_2}}{d\tilde{y}} \right|_{\tilde{y}=tpb}}_{U_{CO,elec}^c} \quad (7)$$

It is shown in Equation (7) that the utilization of carbon monoxide due to the RWGS reaction is directly proportional to the thickness of the cathode current collector ($U_{CO,RWGS}^c \sim \delta^c$), while CO₂ER is inversely proportional ($U_{CO,elec}^c \sim (\delta^c)^{-1}$). This means that decreasing the thickness of the cathode current collector reduces the contribution of the RWGS reaction, while doing so promotes CO₂ER. In extreme cases when $\delta^c \rightarrow 0$, the contribution of heterogeneous chemical reactions in the cathode current collector to the production of carbon monoxide are effectively eliminated ($U_{CO,RWGS}^c \rightarrow 0$), leaving only CO₂ER to produce carbon monoxide.

To further clarify the above conclusion, we evaluate the ratio of the RWGS reaction rate to that of CO₂ER (see Supplementary Note S2 for detailed derivation), in order to obtain the following dimensionless parameter [27,28]:

$$\Gamma_{RWGS}^c \equiv \frac{k_{RWGS}^c R^2 T^2 c_{tot}^{c,in} (\delta^c)^2}{D_{CO_2}} = \frac{\text{reverse water gas shift reaction rate}}{\text{rate of carbon dioxide electro-reduction}} \quad (8)$$

Values of $\Gamma_{RWGS}^c \ll 1$ indicate the RWGS reaction is negligible ($U_{CO,RWGS}^c \sim 0$), resulting in only CO₂ER, while values of $\Gamma_{RWGS}^c \sim 1$ suggest that both processes occur at approximately the same rate. We compare the experimental data from various studies to determine their resultant value of Γ_{RWGS}^c , which are illustrated in Figure 2. The studies in which $\Gamma_{RWGS}^c \ll 1$ (i.e., CO₂ER dominant regime) illustrate that the co-electrolysis and pure steam electrolysis polarization curves overlap each other, while studies with values of $\Gamma_{RWGS}^c \sim 1$ (i.e., mixed CO₂ER and RWGS reaction regime) demonstrate that the co-electrolysis polarization curve lies between pure steam and pure carbon dioxide electrolysis. This approach demonstrates that dimensionless parameter Γ_{RWGS}^c can effectively characterize the behaviour of SOco-ECs with different geometries (button cells versus cell stacks) and operating conditions, and is relevant for all cathode current collector materials and microstructural properties due to its dimensionless nature.

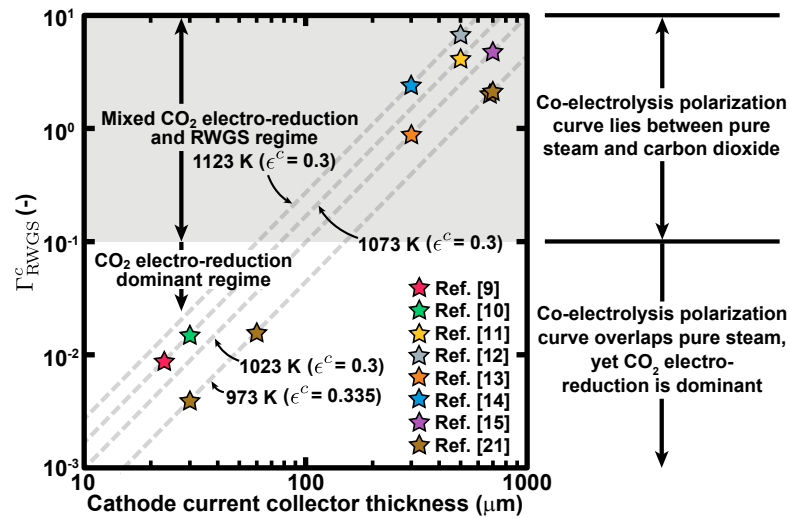


Figure 2. Ratio of the RWGS reaction rate to the rate of CO₂ER, Γ_{RWGS}^c , as a function of the cathode current collector thickness, δ^c , from four different experiments with references shown. The white region corresponds to the regime in which CO₂ER is dominant in comparison to the RWGS reaction ($\Gamma_{RWGS}^c \ll 1$), resulting in overlap between the co-electrolysis and pure steam electrolysis polarization curves (see Refs. [9,10,21]). The gray region represents contributions from both CO₂ER and the RWGS reaction to the production of carbon monoxide ($\Gamma_{RWGS}^c \sim 1$), which causes the co-electrolysis polarization curve to lie between those of pure steam electrolysis and pure carbon dioxide electrolysis (see Refs. [11–15,21]).

Thus far, we have proven that the RWGS reaction and other possible heterogeneous chemical reactions are inconsequential to the transport behaviour of SOco-ECs when the cathode current collector's thickness is sufficiently thin, which in turn promotes CO₂ER for the production of carbon monoxide, and is contrary to what has been proposed in previous analyses [9,10,21]. However, this finding alone does not explain why the polarization curves of both co-electrolysis and pure steam electrolysis overlap one another for sufficiently thin cathodes (i.e., $\Gamma_{RWGS}^c \ll 1$). To explain this phenomenon, we now shift our attention to the thermodynamics of the system, and subsequently Butler-Volmer kinetics for a comparison of the rates of CO₂ER and H₂OER.

2.2. Thermodynamics of Solid Oxide Co-Electrolysis

The rate of work required for the CO₂ER and H₂OER reactions is determined by the product of the operating current and operating potential, according to:

$$\dot{W} = EI \quad (9)$$

and the operating current is proportional to the sum of the rate at which the CO₂ER and H₂OER reactions occur, which is expressed as:

$$I = 2F \left(U_{H_2O,elec}^c J_{H_2O}^{c,in} + U_{CO_2,elec}^c J_{CO_2}^{c,in} \right) \quad (10)$$

Here, $U_{H_2O,elec}^c$ and $U_{CO_2,elec}^c$ represent the electrochemical utilization factors of steam and carbon dioxide, respectively. Additionally, the rate of work for this system, based on the first and second laws of thermodynamics (see Supplementary Note S3 for the derivation), can be expressed as:

$$\dot{W} = U_{H_2O,elec}^c J_{H_2O}^{c,in} \Delta_r g_{H_2O} + U_{CO_2,elec}^c J_{CO_2}^{c,in} \Delta_r g_{CO_2} \quad (11)$$

where $\Delta_r g_{\text{H}_2\text{O}}$ and $\Delta_r g_{\text{CO}_2}$ are the Gibbs free energy required to facilitate the H_2OER and CO_2ER reactions. By substituting Equations (10) and (11) into Equation (9) and solving for the operating potential, we obtain:

$$E = \frac{\zeta_{\text{H}_2\text{O}} \Delta_r g_{\text{H}_2\text{O}} + \zeta_{\text{CO}_2} \Delta_r g_{\text{CO}_2}}{2F} \quad (12)$$

In Equation (12), $\zeta_{\text{H}_2\text{O}}$ and ζ_{CO_2} represent the ratios of the rate of electrochemical utilization of steam and carbon dioxide, respectively, to the total rate of the electrochemical conversion of both, which are expressed as:

$$\zeta_{\text{H}_2\text{O}} = \frac{U_{\text{H}_2\text{O},elec}^c J_{\text{H}_2\text{O}}^{c,in}}{U_{\text{H}_2\text{O},elec}^c J_{\text{H}_2\text{O}}^{c,in} + U_{\text{CO}_2,elec}^c J_{\text{CO}_2}^{c,in}} \quad (13)$$

and:

$$\zeta_{\text{CO}_2} = \frac{U_{\text{CO}_2,elec}^c J_{\text{CO}_2}^{c,in}}{U_{\text{H}_2\text{O},elec}^c J_{\text{H}_2\text{O}}^{c,in} + U_{\text{CO}_2,elec}^c J_{\text{CO}_2}^{c,in}} \quad (14)$$

respectively. Assuming there are equal inlet molar flow rates of carbon dioxide and steam supplied to the system ($J_{\text{H}_2\text{O}}^{c,in} = J_{\text{CO}_2}^{c,in}$), which is often the case, Equations (13) and (14) are further simplified to:

$$\zeta_{\text{H}_2\text{O}} = \frac{U_{\text{H}_2\text{O},elec}^c / U_{\text{CO}_2,elec}^c}{U_{\text{H}_2\text{O},elec}^c / U_{\text{CO}_2,elec}^c + 1} \quad (15)$$

and:

$$\zeta_{\text{CO}_2} = \frac{1}{U_{\text{H}_2\text{O},elec}^c / U_{\text{CO}_2,elec}^c + 1} \quad (16)$$

It is shown in Equations (15) and (16) that if the electrochemical utilization of steam is much higher than that of carbon dioxide ($U_{\text{H}_2\text{O},elec}^c \gg U_{\text{CO}_2,elec}^c$), then $\zeta_{\text{H}_2\text{O}} \rightarrow 1$ and $\zeta_{\text{CO}_2} \rightarrow 0$, causing the operating potential of co-electrolysis in Equation (12) to converge towards that of pure steam electrolysis ($E \approx \Delta_r g_{\text{H}_2\text{O}} / 2F$). Conversely, if $U_{\text{H}_2\text{O},elec}^c \ll U_{\text{CO}_2,elec}^c$, then $\zeta_{\text{H}_2\text{O}} \rightarrow 0$ and $\zeta_{\text{CO}_2} \rightarrow 1$, and the operating potential will overlap that of pure CO_2ER . Based on experiments which have shown the polarization curves of co-electrolysis and pure steam electrolysis to overlap each other [9,10], it is expected the electrochemical utilization of steam is significantly higher than that of carbon dioxide ($U_{\text{H}_2\text{O},elec}^c \gg U_{\text{CO}_2,elec}^c$), and below we provide an explanation for why this is the case.

2.3. Electrochemical Kinetics and Mass Transport

In order to compare the electrochemical utilization factor and kinetics of steam and carbon dioxide, we need to apply the Butler-Volmer equation to both components. For an infinitesimally thin active catalyst layer, the Butler-Volmer equation can be expressed as a boundary condition:

$$i_i = n_i F D_i \left. \frac{dc_i}{dy} \right|_{y=tpb} = n_i F c_i|_{y=tpb} k_i \lambda \left[\exp\left(\frac{\alpha_i n_i F}{RT} \eta_i^c\right) - \exp\left(\frac{-(1-\alpha_i) n_i F}{RT} \eta_i^c\right) \right] \quad (17)$$

where n_i is the number of electrons transferred in electrochemical reaction i , η_i^c is the cathode activation overpotential, α_i is the charge transfer coefficient, λ is the cathode triple phase boundary length, and k_i is the electrochemical reaction rate constant of either steam or carbon dioxide. Substituting the above dimensionless parameters into Equation (17) produces the following expression:

$$\left. \frac{d\tilde{c}_i}{d\tilde{y}} \right|_{\tilde{y}=tpb} = \frac{\delta^c \lambda k_i}{D_i} \tilde{c}_i|_{\tilde{y}=tpb} \left[\exp\left(\frac{\alpha_i n_i F}{RT} \eta_i^c\right) - \exp\left(\frac{-(1-\alpha_i) n_i F}{RT} \eta_i^c\right) \right] \quad (18)$$

which can then be substituted into the electrochemical utilization factor of steam:

$$U_{\text{H}_2\text{O},elec}^c = \frac{LD_{\text{H}_2\text{O}}}{Hc\bar{V}^{c,in}\delta^c\bar{c}_{\text{H}_2\text{O}}^{c,in}} \left. \frac{d\tilde{c}_{\text{H}_2\text{O}}}{d\tilde{y}} \right|_{\tilde{y}=tpb} \quad (19)$$

and that of carbon dioxide:

$$U_{\text{CO}_2,elec}^c = \frac{LD_{\text{CO}_2}}{Hc\bar{V}^{c,in}\delta^c\bar{c}_{\text{CO}_2}^{c,in}} \left. \frac{d\tilde{c}_{\text{CO}_2}}{d\tilde{y}} \right|_{\tilde{y}=tpb} \quad (20)$$

Doing so reveals that the electrochemical utilization factor of steam and carbon dioxide are directly proportional to their respective electrochemical rate constant (i.e., $U_{\text{H}_2\text{O},elec}^c \sim k_{\text{H}_2\text{O}}$ and $U_{\text{CO}_2,elec}^c \sim k_{\text{CO}_2}$). Previous studies have demonstrated that $k_{\text{H}_2\text{O}}$ can be up to 3-times higher than that of carbon dioxide [29,30], while Liang et al. [11] recently found that it can be up to 9-times higher. This correspondingly increases $U_{\text{H}_2\text{O},elec}^c$ over $U_{\text{CO}_2,elec}^c$, increases $\zeta_{\text{H}_2\text{O}}$ while decreasing ζ_{CO_2} (see Equations (15) and (16)), and therefore causes the operating potential of co-electrolysis to approach that of pure steam electrolysis ($E \approx \Delta_r g_{\text{H}_2\text{O}}/2F$). Additionally, given the enhanced mass transport characteristics of steam versus carbon dioxide, in tandem with hydrogen's increased capacity to diffuse from the triple phase boundary in comparison to that of carbon monoxide, the concentration of steam at the triple phase boundary will be higher than that of carbon dioxide ($\tilde{c}_{\text{H}_2\text{O}}|_{\tilde{y}=tpb} > \tilde{c}_{\text{CO}_2}|_{\tilde{y}=tpb}$). This further promotes the electrochemical utilization of steam over carbon dioxide (i.e., $U_{\text{H}_2\text{O},elec}^c \sim \tilde{c}_{\text{H}_2\text{O}}|_{\tilde{y}=tpb}$ versus $U_{\text{CO}_2,elec}^c \sim \tilde{c}_{\text{CO}_2}|_{\tilde{y}=tpb}$) and causes the co-electrolysis polarization curve to coincide with that of pure steam electrolysis, which has been reported in previous experiments [9,10].

In summary, for sufficiently thin cathodes (i.e., $\Gamma_{\text{RWGS}}^c \ll 1$), we find that H₂OER is dominant over CO₂ER, causing the co-electrolysis polarization curve to overlap with that of pure steam electrolysis. Additionally, implementing a thin cathode makes the contribution of the RWGS reaction to the production of carbon monoxide negligible, while promoting CO₂ER (i.e., $U_{\text{H}_2\text{O},elec}^c \gg U_{\text{CO}_2,elec}^c \gg U_{\text{CO,RWGS}}^c$). This analysis enables designers and researchers to select an appropriate value for the thickness of the cathode current collector, in order to exploit a desired reaction pathway to improve the performance and product selectivity of SOco-ECs.

3. Conclusions

This work has provided evidence for the fact that the RWGS reaction is not the reaction pathway responsible for CO generation when the polarization curves of co-electrolysis and pure steam electrolysis coincide with each other. Using dimensional analysis, we demonstrated that reducing the cathode current collector thickness diminishes the contribution of the RWGS reaction, while doing so promotes CO₂ER. We also showed that the RWGS reaction is negligible for sufficiently thin cathode current collectors, which is opposite to what was concluded in previous studies [9,10,21]. We have also derived a dimensionless parameter that characterizes the behaviour of SOco-ECs observed in previous experiments. Furthermore, we have utilized the first and second laws of thermodynamics, coupled with the enhanced electrochemical kinetics and mass transport properties of steam in comparison to carbon dioxide, to determine why the polarization curves of both co-electrolysis and pure steam electrolysis overlap one another. We found that the faster kinetics of H₂OER over CO₂ER, in tandem with CO₂ER being dominant in comparison to the RWGS reaction for sufficiently thin cathode current collectors, cause the pure steam electrolysis and co-electrolysis polarization curves to coincide. The goals of this analysis are to develop an improved understanding of the transport phenomena that govern the performance of SOco-ECs, and to illustrate the value of dimensional analysis when investigating such systems.

Supplementary Materials: The following supporting information can be downloaded at: <https://www.mdpi.com/article/10.3390/en16155781/s1>, Note S1: Evaluation of the effective diffusion coefficient of carbon dioxide in the cathode current collector; Table S1: Cathode current collector thickness, porosity, temperature, effective diffusion coefficient, resultant Γ_{RWGS}^c value, and operating regime for each study examined herein; Note S2: Derivation of dimensionless parameter Γ_{RWGS}^c ; Note S3: Derivation of the rate of work from the first and second laws of thermodynamics.

Author Contributions: Conceptualization, A.S.N. and O.S.B.; methodology, A.S.N.; software, A.S.N.; validation, A.S.N.; formal analysis, A.S.N.; investigation, A.S.N.; writing—original draft preparation, A.S.N.; writing—review and editing, A.S.N., B.A.P. and O.S.B.; visualization, A.S.N.; supervision, B.A.P. and O.S.B.; funding acquisition, O.S.B. All authors have read and agreed to the published version of the manuscript.

Funding: A.S.N. gratefully acknowledges the funding support from a Natural Sciences and Engineering Research Council of Canada (NSERC) Postgraduate Scholarship (PGS-D3), and all authors gratefully acknowledge ENERSENSE, Norway and NTNU, Norway (project no. 68024013) for the financial aid of this project.

Data Availability Statement: The data presented in this study are available in the article and Supplementary Material.

Conflicts of Interest: The authors declare no conflict of interest. The funders had no role in the design of the study; in the collection, analyses, or interpretation of data; in the writing of the manuscript; or in the decision to publish the results.

References

1. Liu, F.; Wang, T.; Li, J.; Wei, T.; Ye, Z.; Dong, D.; Chen, B.; Ling, Y.; Shao, Z. Elevated-temperature bio-ethanol-assisted water electrolysis for efficient hydrogen production. *Chem. Eng. J.* **2022**, *434*, 134699. [[CrossRef](#)]
2. Hauch, A.; Küngas, R.; Blennow, P.; Hansen, A.B.; Hansen, J.B.; Mathiesen, B.V.; Mogensen, M.B. Recent advances in solid oxide cell technology for electrolysis. *Science* **2020**, *370*, eaba6118. [[CrossRef](#)] [[PubMed](#)]
3. Yang, Y.; Tong, X.; Hauch, A.; Sun, X.; Yang, Z.; Peng, S.; Chen, M. Study of solid oxide electrolysis cells operated in potentiostatic mode: Effect of operating temperature on durability. *Chem. Eng. J.* **2021**, *417*, 129260. [[CrossRef](#)]
4. Kamkeng, A.D.; Wang, M. Long-term performance prediction of solid oxide electrolysis cell (SOEC) for CO₂/H₂O co-electrolysis considering structural degradation through modelling and simulation. *Chem. Eng. J.* **2022**, *429*, 132158. [[CrossRef](#)]
5. Yu, S.B.; Lee, S.H.; Mehran, M.T.; Hong, J.E.; Lee, J.W.; Lee, S.B.; Park, S.J.; Song, R.H.; Shim, J.H.; Shul, Y.G.; et al. Syngas production in high performing tubular solid oxide cells by using high-temperature H₂O/CO₂ co-electrolysis. *Chem. Eng. J.* **2018**, *335*, 41–51. [[CrossRef](#)]
6. Technology Roadmap: Energy and GHG Reductions in the Chemical Industry via Catalytic Processes. Available online: <https://icca-chem.org/wp-content/uploads/2020/05/Technology-Roadmap.pdf> (accessed on 31 October 2022).
7. Zheng, Y.; Wang, J.; Yu, B.; Zhang, W.; Chen, J.; Qiao, J.; Zhang, J. A review of high temperature co-electrolysis of H₂O and CO₂ to produce sustainable fuels using solid oxide electrolysis cells (SOECs): Advanced materials and technology. *Chem. Soc. Rev.* **2017**, *46*, 1427–1463. [[CrossRef](#)]
8. Zhang, X.; Song, Y.; Wang, G.; Bao, X. Co-electrolysis of CO₂ and H₂O in high-temperature solid oxide electrolysis cells: Recent advance in cathodes. *J. Energy Chem.* **2017**, *26*, 839–853. [[CrossRef](#)]
9. Stoots, C.; O'Brien, J.; Hartvigsen, J. Results of recent high temperature coelectrolysis studies at the Idaho National Laboratory. *Int. J. Hydrogen Energy* **2009**, *34*, 4208–4215. [[CrossRef](#)]
10. Kim-Lohsoontorn, P.; Bae, J. Electrochemical performance of solid oxide electrolysis cell electrodes under high-temperature coelectrolysis of steam and carbon dioxide. *J. Power Sources* **2011**, *196*, 7161–7168. [[CrossRef](#)]
11. Liang, J.; Wang, Y.; Zhu, J.; Han, M.; Sun, K.; Sun, Z. Investigation on the reaction mechanism of solid oxide co-electrolysis with different inlet mixtures based on the comparison of CO₂ electrolysis and H₂O electrolysis. *Energy Convers. Manag.* **2023**, *277*, 116621. [[CrossRef](#)]
12. Zhang, W.; Zheng, Y.; Yu, B.; Wang, J.; Chen, J. Electrochemical characterization and mechanism analysis of high temperature Co-electrolysis of CO₂ and H₂O in a solid oxide electrolysis cell. *Int. J. Hydrogen Energy* **2017**, *42*, 29911–29920. [[CrossRef](#)]
13. Ebbesen, S.D.; Knibbe, R.; Mogensen, M. Co-Electrolysis of Steam and Carbon Dioxide in Solid Oxide Cells. *J. Electrochem. Soc.* **2012**, *159*, F482. [[CrossRef](#)]
14. Graves, C.; Ebbesen, S.D.; Mogensen, M. Co-electrolysis of CO₂ and H₂O in solid oxide cells: Performance and durability. *Solid State Ion.* **2011**, *192*, 398–403. [[CrossRef](#)]
15. Li, W.; Wang, H.; Shi, Y.; Cai, N. Performance and methane production characteristics of H₂O–CO₂ co-electrolysis in solid oxide electrolysis cells. *Int. J. Hydrogen Energy* **2013**, *38*, 11104–11109. [[CrossRef](#)]

16. Aicart, J.; Laurencin, J.; Petitjean, M.; Dessemond, L. Experimental Validation of Two-Dimensional H₂O and CO₂ Co-Electrolysis Modeling. *Fuel Cells* **2014**, *14*, 430–447. [[CrossRef](#)]
17. Luo, Y.; Shi, Y.; Li, W.; Cai, N. Comprehensive modeling of tubular solid oxide electrolysis cell for co-electrolysis of steam and carbon dioxide. *Energy* **2014**, *70*, 420–434. [[CrossRef](#)]
18. Ni, M. 2D thermal modeling of a solid oxide electrolyzer cell (SOEC) for syngas production by H₂O/CO₂ co-electrolysis. *Int. J. Hydrogen Energy* **2012**, *37*, 6389–6399. [[CrossRef](#)]
19. Ni, M. An electrochemical model for syngas production by co-electrolysis of H₂O and CO₂. *J. Power Sources* **2012**, *202*, 209–216. [[CrossRef](#)]
20. Li, W.; Shi, Y.; Luo, Y.; Cai, N. Elementary reaction modeling of solid oxide electrolysis cells: Main zones for heterogeneous chemical/electrochemical reactions. *J. Power Sources* **2015**, *273*, 1–13. [[CrossRef](#)]
21. Li, W.; Shi, Y.; Luo, Y.; Cai, N. Elementary reaction modeling of CO₂/H₂O co-electrolysis cell considering effects of cathode thickness. *J. Power Sources* **2013**, *243*, 118–130. [[CrossRef](#)]
22. Xu, H.; Chen, B.; Irvine, J.; Ni, M. Modeling of CH₄-assisted SOEC for H₂O/CO₂ co-electrolysis. *Int. J. Hydrogen Energy* **2016**, *41*, 21839–21849. [[CrossRef](#)]
23. Menon, V.; Fu, Q.; Janardhanan, V.M.; Deutschmann, O. A model-based understanding of solid-oxide electrolysis cells (SOECs) for syngas production by H₂O/CO₂ co-electrolysis. *J. Power Sources* **2015**, *274*, 768–781. [[CrossRef](#)]
24. Beale, S.B.; Andersson, M.; Boigues-Muñoz, C.; Frandsen, H.L.; Lin, Z.; McPhail, S.J.; Ni, M.; Sundén, B.; Weber, A.; Weber, A.Z. Continuum scale modelling and complementary experimentation of solid oxide cells. *Prog. Energy Combust. Sci.* **2021**, *85*, 100902. [[CrossRef](#)]
25. Ni, M. Modeling of a solid oxide electrolysis cell for carbon dioxide electrolysis. *Chem. Eng. J.* **2010**, *164*, 246–254. [[CrossRef](#)]
26. Haberman, B.; Young, J. Three-dimensional simulation of chemically reacting gas flows in the porous support structure of an integrated-planar solid oxide fuel cell. *Int. J. Heat Mass Transf.* **2004**, *47*, 3617–3629. [[CrossRef](#)]
27. Nielsen, A.S.; Peppley, B.A.; Burheim, O.S. Tuning transport mechanisms in fuel-assisted solid oxide electrolysis cells for enhanced performance and product selectivity: Thermodynamic and kinetic modeling. *Chem. Eng. J.* **2023**, *452*, 139079. [[CrossRef](#)]
28. Nielsen, A.S.; Peppley, B.A.; Burheim, O.S. Controlling the contribution of transport mechanisms in solid oxide co-electrolysis cells to improve product selectivity and performance: A theoretical framework. *Appl. Energy* **2023**, *344*, 121301. [[CrossRef](#)]
29. Matsuzaki, Y.; Yasuda, I. Electrochemical Oxidation of H₂ and CO in a H₂-H₂O-CO-CO₂ System at the Interface of a Ni-YSZ Cermet Electrode and YSZ Electrolyte. *J. Electrochem. Soc.* **2000**, *147*, 1630. [[CrossRef](#)]
30. Sukeshini, A.M.; Habibzadeh, B.; Becker, B.P.; Stoltz, C.A.; Eichhorn, B.W.; Jackson, G.S. Electrochemical Oxidation of H₂, CO, and CO/H₂ Mixtures on Patterned Ni Anodes on YSZ Electrolytes. *J. Electrochem. Soc.* **2006**, *153*, A705. [[CrossRef](#)]

Disclaimer/Publisher’s Note: The statements, opinions and data contained in all publications are solely those of the individual author(s) and contributor(s) and not of MDPI and/or the editor(s). MDPI and/or the editor(s) disclaim responsibility for any injury to people or property resulting from any ideas, methods, instructions or products referred to in the content.